HYDROTALCITE-LIKE COMPOUNDS: A WAY TO RECOVER A HAZARDOUS WASTE IN THE ALUMINIUM TERTIARY INDUSTRY

R. Galindo[a], A. López-Delgado[a*], I. Padilla[a] and M. Yates[b]

[a]National Centre for Metallurgical Research, CSIC. Avda./ Gregorio del Amo, 8.

28040 Madrid, Spain

[b]Institute of Catalysis and Petrochemistry, CSIC. C./ Marie Curie, 2.

28049 Madrid, Spain

*Author to whom correspondence should be addressed: alopezdelgado@cenim.csic.es

Abstract

Magnesium-aluminium hydrotalcite-like compounds at ratios of 2:1, 3:1 and 4:1 were prepared using a non-conventional aluminium source, the hazardous wastes from the aluminium tertiary industry. The method consisted in a conventional coprecipitation at constant pH 10 with magnesium chloride hexahydrate and stable solutions of Al^{3+} from dispersions of the fine powder from the sleeve filter suction system in the aluminium slag milling process. Resulting materials were strongly dependent on the presence of iron in the layers, as well as the carbonate-chloride content in the interlayer which affected the final properties. XRD and SAED indicated low crystallinity for these materials. Furthermore, as can be seen by SEM, the formation of disordered tiny nuclei was significant causing small spherical agglomerates. The infrared spectra showed a change of symmetry in the interlayer for the different ratios and the textural data suggested the "ink-bottle shaped" mesopores and type IIb isotherms, similar to the

1

results obtained for pillared clays, and the transition to H2 type in the hysteresis loops as function of the higher ratio.

Keywords: Hydrotalcite; layered double hydroxide (LDH); non-conventional aluminium source; hazardous waste;

1. Introduction

Hydrotalcite-like compounds are a valuable and widely reported group of materials with complex structure that are composed of positively charged brucite-like layers $[M_{1-x}^{2+} M_x^{3+} (OH)_2]^{x+}$, where M^{2+} and M^{3+} are divalent and trivalent cations distributed among octahedral positions, alternating with disordered and negatively charged interlayers $[A_{x/n}]^{n-}$ formed for instance by inorganic ions, heteropolyacids, organic acids, *etc*. [**Miyata, 1983, Cavani et al., 1991**] which present a formula of type $[M_{1-x}^{2+} M_x^{3+} (OH)_2]^{x+} [A_{x/n}]^{n-} \cdot mH_2O$. The presence of the different anions located in the interlayer region leads to distinct interlayer thicknesses which play an important role when ion exchange is desired. Furthermore, under thermal decomposition, these materials can produce stable non-stoichiometric mixed metal oxides which possess homogeneous dispersion of the elements, high specific surface areas and strong basic properties. Moreover, the "memory effect" allows the reconstruction, under mild conditions, of the original hydrotalcite structure when the calcined product contacts with a solution containing anions. These special features enable a huge number of applications with high added-value in several fields such as heterogeneous catalysts, adsorbents, flame retardants, ion exchangers, drug releasers, anticorrosives, *etc*. [**Choudary et al., 2000,**

Constantino et al., 2008, Yang et al., 2013]. Nowadays, many methods have been described in the literature for preparing these materials. In general, they refer to conventional coprecipitation by slow addition, and simultaneously under stirring, of metal nitrates/chlorides as well as precipitants (sodium hydroxide, ammonia, urea, *etc.*) at a fixed pH (usually from 8 to 13), or increasing the basicity of the metal solution to the corresponding pH value, followed by a long ageing time (about 1 day or more) and/or hydrothermal treatment in order to improve the crystallinity at temperatures from 60 to 140ºC; or unconventional procedures, like ultrasound assisted coprecipitation methods or ageing for instance by microwave radiation [**Climent et al., 2004, Okamoto et al., 2007, Yang et al., 2007**]. Since the control of textural characteristics such as particle size, porosity or degree of crystallinity leads to satisfy new requirements, other authors also have reported sol-gel synthesis, doping with other elements, use of surfactants and studies with microemulsions or micelles [**Othman et al., 2006, Pérez Bernal et al., 2009, Bellezza et al., 2012, Schulze et al., 2001**] with the objective of establishing a better control on the synthesis parameters and improve the resulting properties for these materials.

The slag milling process performed by the aluminium tertiary industry generates hazardous wastes whose handling is regulated by the Directive 2008/98/EC in the European Union. Briefly, the scope of this Directive is to prevent or reduce waste generation and promote the recovery as well as its use. Particularly, considers that a hazardous waste may not be considered as non-hazardous, only by dilution to levels below the thresholds values, and encourages the study of innovative re-using ways. Thus, a significant number of investigations have dealt with the recycling of hazardous wastes in order to increase their value in a whole range of activities and fields. With

regards of these points, only a few papers have focused on the aluminium tertiary industry. Furthermore, authors have been concerned with recovery capabilities as aluminium precursors to obtain added-value materials, and have described waste as a complex and heterogeneous blend of several components such as corundum, spinels, aluminium nitride (in high content, from 10 to 25% in mass), metallic aluminium, quartz, calcite, iron oxide, also other minor oxides and salts [**López-Delgado and Tayibi, 2012, López-Delgado et al., 2012**]. The high content of aluminium nitride, and the presence of sulphide, can initiate a simple reaction with moisture in air, releasing ammonia and hydrogen sulphide as toxic by-products in the environment [**Krnel et al., 2004**].

In this context, few examples for procedures of the hydrotalcite obtain by using wastes as precursors are documented in the literature. For instance, Kuwahara [**Kuwahara et al., 2010**] described appropriately the use of blast furnace slags (BFS) as a source for the synthesis of hydrotalcite-like compounds, and zeolites. Thus in relation to this substance, authors referred BFS as a commercial waste, however, they alert about new ways of recycling due to the high increasing production which is more intense than its consumption. In fact, a lot of countries, including the European Union, consider the blast furnace slag as a by-product instead of an inert or hazardous waste [**COM(2007) 59 final, 2007**]. Murayama [**Murayama et al., 2006**] prepared hydrotalcite from aluminium dross which were discharged in an aluminium secondary industry and evaluated its catalytic properties. The use of bauxite residue, a by-product of the Bayer process, as a precursor for the synthesis has also been reported [**Santini and Fey, 2012**].

Therefore, the aim of this work was to acquire a better understanding about the preparation and characterisation of hydrotalcites by the coprecipitation method using an alternative aluminium source as wastes. The synthesis was developed at constant and controlled pH 10. For this purpose, two samples of hazardous wastes, generated by the aluminium slag milling process in the tertiary industry and destination to secure landfill, were treated separately to provide stable aluminium solutions. These solutions were employed as precursors combined with magnesium chloride in order to obtain Mg-Al-hydrotalcites with a variable ratio. The resulting materials were characterised by several techniques such as XRD, FT-IR, DTA-TG, SEM and TEM. The specific surface area (SSA), zeta-potential and isoelectric points were also determined to complete the textural characterisation of samples.

2. Experimental

2.1. Reagents

The Mg/Al chloride-carbonated hydrotalcites produced in this study were based on Mg/Al ratios of 2:1, 3:1 and 4:1. In order to prepare these materials, magnesium chloride hexahydrate (Mg^{2+} precursor, reagent grade), and 1 mol/l sodium hydroxide (precipitant reagent) supplied by Panreac S.A were used. The demanded Al^{3+} was provided by hazardous aluminium waste (samples denoted as P6 and P9) from a tertiary industry (Metalquex, S.L. - Zaragoza, Spain). This waste was the fine powder which came from the sleeve filter suction system in the aluminium slag milling process. Thus, the Al^{3+} precursor consisted of an aluminium solution which was obtained by the

5

process described by Gonzalo-Delgado [**Gonzalo-Delgado et al., 2011**]. Briefly, 20 g sample of powdery waste was dispersed in a 200 ml hydrochloric aqueous solution (10% v/v) for 3 hours at 80ºC under vigorous stirring. Then, solution was separated from solid by filtering on a GTTP Millipore filter of 0.22 µm at 5 bars pressure. The resulting solution was adjusted to 500 ml with distilled water. Solutions were colourless or yellowish depending on the presence of other minor components such as iron. At the end, metal concentrations, Mg^{2+} as well as Al^{3+}, were analysed by Atomic Absorption Spectroscopy (AAS), on a Varian SpectrAA 220 FS, to calculate the theoretical concentrations required for the three different ratios. Furthermore, aluminium chloride hexahydrate (reagent grade) as precursor, supplied by Panreac S.A, was used to prepare blank materials for comparison (samples denoted as BL).

2.2. Hydrotalcite synthesis

Hydrotalcites were synthesised by the coprecipitation method for 2 hours at 70 ºC. For this purpose, a 200 ml of Al^{3+} and Mg^{2+} mixed aqueous solution at the Mg/Al required ratio was added drop wise to a stirred solution, at fixed pH 10, composed of 400 ml of distilled water and 1 mol/l NaOH. To maintain the pH value of this blend during the addition of metals, more of the diluted sodium hydroxide was titrated. In the meantime, a fine white-yellowish solid dispersion was observed. Upon titration, the final volume was adjusted to 800 ml with distilled water and then, the dispersion was aged at 70 ºC for 18 hours under constant stirring. The resulting solid material was separated by filtration under pressure (at 5 bars) on a GTTP Millipore filter of 0.22 µm and washed thrice with 500 ml of basic distilled water (pH 9-10) to remove chlorides and other unreacted substances. Finally, the cake was dried in air at 80 ºC for 24 h and manually

grounded with a mortar. The presence of carbonate was expected due to the system not being purged with N_2 and reagents not being CO_2 free. ICP-OES was performed to confirm the final Mg/Al ratio in all samples (measurement of 0.1 g of hydrotalcite synthesised in 100 ml aqueous HCl 10% v/v) on a Perkin Elmer Optima 3300DV.

2.3. Waste and sample characterisation

Wastes were analysed by X-ray fluorescence (XRF), in order to determine their main chemical composition. Analyses were performed on a Philips PW1480 wavelength-dispersive X-ray fluorescence spectrometer with a dual target Mo/Sc X-ray tube at 80 kV and 35 mA, using fusion disks prepared with lithium tetraborate. In addition, contents of aluminium nitride present in wastes were calculated from the Kjeldhal method by means of a steam distillation system provided by Velp Scientifica. Results from these analyses are shown in Table 1. Moreover, Figure 1 shows XRD spectra obtained with the main phase assignments. As can be seen, a high content of aluminium nitride phase was present combined with metallic aluminium and corundum. Furthermore, reflections of halite (NaCl) and spinel $MgAl_2O_4$ were intense. A more complete and accurate phase identification was unfeasible due to the high background effect and number of low intensity reflections.

Samples were characterised as follows. Powder X-ray diffraction (XRD) was carried out using a Bruker D8 Advance diffractometer with Cu Kα radiation, from 4 to 70 º2θ, at a scan rate of 0.02 º2θ, 8 s per step, 40 kV and 30 mA. Fourier-transform infrared (FT-IR) spectra were recorded under vacuum on a Bruker IFS 66v/S in the range of 250-4000 cm^{-1} by means of transmission measurements from sample diluted in KBr.

TDA-TG was performed up to 800 ºC in an air atmosphere (flow rate 100 ml/min), at a ramp of 10 ºC/min, on a SDT-Q600 by TA Instruments. In this technique, alumina crucibles were filled with 10 mg of sample. The morphological features of the representative samples were analysed by Scanning Electron Microscopy (SEM) using a Hitachi S4800 (15.0 kV, 14.8 mm) equipped with an Energy Dispersive X-ray Detector (EDS) supplied by Oxford (samples were coated with graphite by sputtering procedure before SEM-EDS studies), as well as, Transmission Electron Microscopy (TEM) and Electron Diffraction patterns (SAED) which were performed on a JEOL 2010 (200 kV) that allowed the determination of the internal structure of these materials. Zeta-potentials and isoelectric points (IEP) were measured using a Malvern ZetaSizer Nano ZS. Textural characterisation of samples was carried out by determination of nitrogen adsorption/desorption isotherms at 77 K on samples previously outgassed overnight at 300 °C [**Fetter et al., 2000**] to ensure that they were free of any loosely adsorbed species during measurement. The specific surface area (SSA) was determined from the adsorption branch of the isotherms in the linear part of the BET plot, usually located in relative pressures of 0.05 to 0.3 for non-microporous materials, and 0.02 to 0.12 for microporous ones. The microporosity was determined from a t-plot analysis, using the Harkins-Jura equation for the thickness of the adsorbed layer at each relative pressure. From the slope of this line, the external area (S_{EXT}), that is the area not involved in the filling of micropores, was determined. The volume adsorbed at the intercept was used to calculate the micropore volume. The amount adsorbed on the desorption branch of the isotherm at a relative pressure of 0.96 was taken as the pore volume in pores of less than 50 nm pore diameter, that is the micro and mesoporosity. A model ASAP2020 supplied by Micromeritics, surface area and porosimetry analyzer, was used to acquire this textural information.

3. Results and discussion

3.1. Characterisation of the resulting materials

XRD was performed to ensure the presence of the hydrotalcite phase. Figure 2 shows the X-ray patterns corresponding to both blanks and samples prepared with aluminium waste P6 and P9, at ratios 2:1 (Fig. 2a), 3:1 (Fig. 2b) and 4:1 (Fig. 2c). Plots revealed an incomplete development for the hydrotalcite reflections in all cases, which implied a low crystallinity, especially for samples prepared from wastes. No impurity phases were observed. However, the growing presence of iron and other minor components with different ionic radii compared to Mg^{2+} and Al^{3+}, in Al^{3+} precursors, increased this situation that could be attributed to their incorporation into the hydrotalcite phase. In this context, samples synthesised from P6 waste presented the lowest crystallinity, suggesting that impurities such as iron (highest content) would be entering the structure, at least as dopants. In addition, the positions of reflections and their relative intensities revealed more similarities to carbonated hydrotalcites than chlorided ones. The comparison between ratios showed an increasing crystallinity until ratio 3:1, afterwards this feature was reduced. The crystallite size (D) determined by the Scherrer equation considering the 003 basal reflection for samples and parameters *a* and *c* of the layered structure are reflected on Table 2. The *a* parameter is associated with the average cation-cation distance within the layers and *c* is related to the thickness of the brucite-like layer and the interlayer distance [**Pérez-Ramírez et al., 2001**]. As can be seen, *a* and *c* parameters grew for higher ratios Mg/Al due to less incorporation of Al^{3+} cations into the brucite layers. The Al^{3+} crystal radius in octahedral coordination (0.675 Å) is

9

smaller than Mg^{2+} (0.86 Å) as a result, distances among layers and cations were reduced [**Shannon, 1976**]. The comparison of values between blanks and waste samples showed that both *a* and *c* parameters suffered a variation. In general, wastes presented minor values for cell parameters in all ratios, showing that dopant elements were present.

The FT-IR spectra are plotted in Figures 3 and 4. Figure 3 compares references (BL) at the three ratios with the respective samples obtained from wastes P6 and P9. Figure 4 shows the differences obtained between the distinct ratios, exemplified only for the blank series. As can be seen from these plots, spectra for wastes were similar to blanks and revealed the typical spectrum for hydrotalcites [**Kloprogge et al., 2004, Hernández-Moreno et al., 1985**]. At around 3469-3518 cm^{-1}, the metal-OH stretching appeared. The utmost wavenumber obtained corresponded to the higher Mg^{2+} content in the hydrotalcite resembled the band that appears in the brucite spectrum (3570 cm^{-1}). Furthermore, spectra showed overlapping for the 2938 cm^{-1} band (CO_3-H_2O bridging mode) and the 3266 cm^{-1} band (assigned to H-bonded interlayer H_2O surrounding the interlayer anion). The water-bending mode was located within the range of 1624-1634 cm^{-1}. The symmetric stretching v_3 for the CO_3^{2-} presented in the interlayer could be associated with a sharp peak that appeared between 1367-1370 cm^{-1} in the case of ratios 2:1 and 3:1, but for ratio 4:1, this peak turned into a broad doublet (shoulder around 1400-1474 cm^{-1}) that could indicate a more disordered lamellar space because of the greater distance between layers (highest *c* parameter). A band corresponding to bicarbonate anion adsorption at around 1000 cm^{-1}, could be observed that was more intense for samples at ratio 3:1, being attributed to the incorporation of this anion due to rinsing with basic water at pH 9-10 before drying. Below 1000 cm^{-1}, more differences

were observed between spectra. The ratio 2:1 presented 5 bands at 779, 678, 558, 448, 398 cm^{-1}, in contrast, the other ratios overlapped bands and presented only three at 790, 620-583, 412-406 cm^{-1}. These bands corresponded to Mg-OH and Al-OH combined translations. In the case of ratio 2:1, the higher Al^{3+} content generated a major stress in the hydrotalcite structure, and showed less coupling among active modes due to the lower distance between layers as the *c* parameter indicated (higher proximity between cations and interlayer anions). However, the discrimination between Mg-OH and Al-OH in this region of the spectrum was a complex task due to the similar band positions in most cases.

The morphology of samples is shown in Figure 5. In this capture, SEM micrograph corresponding to sample 3P6 represents the appearance obtained for all materials. It was remarkable the presence of small, homogeneous, as well as spherical agglomerates (less than 100 nm in size) which formed aggregates (more than 15 µm in size) due to the high supersaturation level of hydroxyl ions in the basic media during the synthesis. In fact, a fast nucleation process would be induced causing a disordered tiny nuclei generation. Thus, nuclei could adsorb sodium ions onto its surface with no preference, avoiding the metal approaching (Mg^{2+}, Al^{3+}) and the subsequent ordered growth [**Henrist et al., 2003**]. The isoelectric points (IEP) calculated for samples indicated values that exceed 13 (+33 ≤ zeta potential ≤ +44 mV). According to this, there was an elevated residual charge on the surface, and particles were forced to adopt the globular-type structure (instead of the lamellar formation) in order to minimise their surface. Figure 6 shows the TEM micrograph for sample 3P9. This technique confirmed the presence of nanometric spherical agglomerates (less than 10 nm in size) and the absence of crystal definition. Moreover, SAED revealed a non-crystalline order for these

materials and therefore, the amorphous character was significant. EDS indicated that chloride presence in hydrotalcite interlayer was minimal, suggesting that anions in this region were composed basically by carbonate ones trapped during the synthesis process. Furthermore, iron and silicon impurities appeared in low contents about 1% in mass for samples synthesised from waste P6 and 0.5% in mass from waste P9.

DTA-TG results at the three different Mg/Al ratios are plotted in Figure 7. In these graphics, blanks are compared to samples synthesised from wastes P6 and P9. TG showed four distinct ranges in all cases. Firstly, a significant drop located within the range of 50-200 ℃, corresponding to the water lost, both adsorbed and interlayer (two changes in DTA more visible in ratio 2:1; ratio 3:1 and 4:1 have a similar behaviour and overlap these changes). The second region (from 200 to 280-300 ℃) showed a slight decrease corresponding to the OH^- bonded to Al^{3+} that was beginning to disappear [**Vágvölgyi et al., 2008, Stanimirova et al., 1999, Yang et al., 2002**]. As plots indicated, loss in 4:1 was similar to a plateau in comparison to ratio 2:1 due to the amount of Al^{3+} in 4:1 being lower. The upper limit (280-300 ℃) depended on the presence of impurities in the crystalline structure. Thus, P6 samples (highest content in iron) presented a higher value of temperature in comparison to samples from P9 (minor content) and blanks, due to the possibility of bonds between hydroxyl groups and iron. The third region formed a clear endothermic peak in DTA, its minimum was located at 345-387 ℃ and corresponded to the overlapping of the loss of OH^- bonded to Mg^{2+} (break down at low temperatures) and interlayer carbonates (at high temperatures). The position of this peak increased for samples from wastes depending on the higher content of impurities present in the hydrotalcite. P9 samples presented two bands that would correspond to two slow steps in the decarbonation process similar to the process

described by Vágvölgyi [**Vágvölgyi et al., 2008**]. The last region (from 425 to 800ºC) corresponded to the removing of the remaining carbonates and chlorides, leading to the complete collapse of the structure and formation of mixed oxides.

The adsorption isotherms for 2P9, 3P9 and 4BL exhibited the type IIb behaviour, as can be seen in Figure 8. These isotherms are usually found in clay materials. The rest of samples exhibited a less asymptotic behaviour at top P/P^0, being also type IIb with a slight similarity to type IV cause of the incipient plateau. Hysteresis loops suffered a transition from H1/H3 type to H2 as a function of the ratio (according to IUPAC). The 2BL, 2P6 and 3BL samples showed narrow hysteresis loops with nearly parallel adsorption and desorption branches quite similar to H1 type [**Jaroniec et al., 1998**]. In the case of 2P9 sample, the H3 type was remarkable [**Glage et al., 2009**]. As can be seen in Figure 8, there was a deformation in the loops for ratio 3:1, including the presence in 3P6 of two kinds of pores (blocked and open). For ratio 4:1, H2 loops appeared in blank and waste samples. The pore size distribution indicated only the breaking of the nitrogen meniscus at a relative pressure of 0.42 P/Pº for 3BL, 4BL, 4P6 and P9 samples (around 3.7 nm). The pore size distributions for 2BL and 2P6 were centered at 23 nm. In the case of 2P6, the values were located at 3.7 nm and 7.7 nm. These results suggested a connection of ink-bottle pores that were assembled in all samples with random size distributions, both in cavities and necks, as in the case of conventional models. The presence of higher disorder in pores for higher Mg/Al ratio would be related to the corresponding composition and the removal of the hydroxyl bonded to Al^{3+} from the structure at 300ºC. However, a more detailed analysis should be considered in order to analyse phenomena such as capillary condensation and pore blocking/percolation mechanisms [**Grosman and Ortega, 2008**].

Values of textural characterisation are gathered in Table 3. Specific surface area by BET method ranged between 118 and 208 m^2/g. The calculated external surface area (S_{EXT}) presented similar values between blank and samples from P9 waste, and higher values in the case of P6 samples. Micropore volume increased slightly from 2:1 to 3:1 being more significant for the samples coming from wastes. For ratio 4:1, the microporosity was low. The mesopore volume showed a reduction as a function of the ratio, being more considerable in the case of wastes, which would be attributable to a more intense influence of the macroporosity as a consequence of the interaction of gas with the surface of layers.

3.2. The feasibility of industrial-scale production

Calculated values of acid consumption and reused waste are collected in Table 4. As can be seen, significant rates of recovery were observed for wastes, being more than 0.60 kg of waste per kg of synthesized hydrotalcite in the ratio 2:1. The demanded quantities of HCl ranged between 0.76 and 0.42 kg per kg of hydrotalcite. These results could suggest that the use of acid would signify an additional cost for the process; however, the high rate of recovery would balance this fact due to the lowest cost of the waste when is compared with traditional soluble aluminium precursors. The main constraints for the industrial-scale production would focus on the raw materials for the production of Mg^{2+} solution due to the process was performed under mild conditions. In this sense, the use of magnesium chloride would be the key; this precursor is mainly the most expensive. Thus, the substitution of magnesium chloride for magnesium carbonate would signify an important cost reduction for an industrial production.

4. Conclusions and future developments

The synthesis of hydrotalcite-like compounds revealed a simple method for the recovery of the hazardous waste from the aluminium slag milling process that implied both environmental and economical benefits due to the production of a well-known value-added product. Hydrotalcite synthesis was based on a conventional coprecipitation at constant pH 10 using $MgCl_2 \cdot 6H_2O$ and Al^{3+} solutions prepared from the hazardous waste that permitted a controlled releasing of toxic gas (ammonia and sulphide) from the waste into reaction. Resulting materials were affected by different parameters such as the different Mg/Al ratio, the doping in the layers caused mainly by iron (between 0.5 and 1% in mass), as well as the presence of chloride and carbonate in the interlayers. In summary, the crystallinity was low and the cell parameters reduced (both *a* and *c*) as the iron incorporation increased; the carbonate content was high (absence of N_2 atmosphere and use of reagents that were not CO_2 free) displacing the chloride anion despite the higher content for the latter; the symmetry in the interlayer was lower at upper Mg/Al ratios, due to the greater distance between layers; the morphology was small spherical agglomerates that formed aggregates caused by disordered tiny nuclei generation (high Z potential); lower adsorption properties in comparison to blank materials. Data indicated the typical type IIb isotherms and "ink-bottle shaped" mesopores that appeared in adsorbents like pillared clays, with a low pore diameter (3.7nm) and a significant mesopore volume reduction when the Mg/Al ratio was higher. Taking into account these properties, the use of these hydrotalcites as adsorbents would be a viable application with added-value. In this way, a further study for the improvement of the value for these products will be focused on their use as anticorrosive protectors on metal

surfaces with the introduction of anticorrosive inhibitors into the interlayer. Moreover, the observed adsorption properties will be valuable by acting as a barrier for corrosive substances.

Acknowledgements

References

Bellezza F., Nocchetti M., Posati T., Giovagnoli S., Cipiciani A., 2012. Synthesis of colloidal dispersions of NiAl, ZnAl, NiCr, ZnCr, NiFe and MgFe hydrotalcite-like nanoparticles. Journal of Colloid and Interface Science 376: 20-27

Cavani F., Trifirò F., Vaccari A., 1991. Hydrotalcite-type anionic clays: Preparation, properties and applications. Catalysis Today 11: 173-301

Choudary B.M., Lakshimi Kantam M., Venkat Reddy Ch., Aranganathan S., Lakshimi Santhi P., Figueras F., 2000. Mg-Al-O-t-Bu hydrotalcite: a new and efficient heterogeneous catalyst for transesterification. Journal of Molecular Catalysis A: Chemical 159: 411-416

Climent M.J., Corma A., Iborra S., Epping K., Velty A., 2004. Increasing the basicity and catalytic activity of hydrotalcites by different synthesis procedures. Journal of Catalysis 225: 316-319.

Constantino U., Ambrogi V., Nocchetti M., Perioli L., 2008. Hydrotalcite-like compounds: Versatile layered hosts of molecular anions with biological activity. Microporous and Mesoporous Materials 107: 149-160.

COM (2007) 59 final, 2007. Communication from the Commission to the Council and the European Parliament on the interpretative communication on waste and by-products. Commission of the European Communities, Brussels.

Fetter G., Olguín M.T., Bosch P., Bulbulian S., 2000. Surface areas of nitrated hydrotalcites. Journal of Porous Materials 7: 469-473.

Gonzalo-Delgado L., López-Delgado A., López F.A., Alguacil F.J., López-Andrés S., 2011. Recycling of hazardous waste from tertiary aluminum industry in a value-added material. Waste Management and Research 29 (2): 127-134.

Glage A., Ceccato R., Lonardelli I., Girardi F., Agresti F., Principi G., Molinari A., Gialanella S., 2009. A powder metallurgy approach for the production of a MgH_2-Al composite material. Journal of Alloys and Compounds 478: 273-280.

Grosman A. and Ortega C., 2008. Capillary condensation in porous materials. Hysteresis and interaction mechanism without pore blocking/percolation process. Langmuir 24(8): 3977-3986.

Hernández-Moreno M.J., Ulibarri M.A., Rendon J.L., Serna C.J., 1985. IR Characteristics of hydrotalcite-like compounds. Physics and Chemistry of Minerals 12: 34-38.

Henrist C., Mathieu J.-P., Vogels C., Rulmont A., Cloots R., 2003. Morphological study of magnesium hydroxide nanoparticles precipitated in diluted aqueous solution. Journal of Crystal Growth 249: 321-330.

Jaroniec C.P., Jaroniec M., Kruk M., 1998. Comparative studies of structural and surface properties of porous inorganic oxides used in liquid chromatography. Journal of Chromatography A 797: 93-102.

Kloprogge J.T., Hickey L., Frost, R.L., 2004. FT-Raman and FT-IR spectroscopy study of synthetic Mg/Zn/Al-hydrotalcites. Journal of Raman Spectroscopy 35: 967-974.

Krnel K., Drazic G., Kosmac T., 2004. Degradation of AlN powder in aqueous environments. Journal of Materials Research 19 (4): 1157-1163.

Kuwahara Y., Ohmichi T., Kamegawa T., Mori K., Yamashita H., 2010. A novel conversion process for waste slag: synthesis of a hydrotalcite-like compound and zeolite

from blast furnace slag and evaluation of adsorption capacities. Journal of Materials Chemistry 20: 5052-5062.

López-Delgado A., Fillali L., Jiménez J.A., López-Andrés S., 2012. Synthesis of α-alumina from a less common raw material. Journal of Sol-Gel Science and Technology 64: 162-169.

López-Delgado A., Tayibi H., 2012. Can hazardous waste becomes a raw material? The case study of an aluminium residue: a review. Waste Management and Research 30 (5): 474-484.

Miyata S., 1983. Anion Exchange Properties of hydrotalcite-like compounds. Clays and Clay Minerals 31 (4): 305-311.

Murayama N., Shibata J., Sakai K., Nakayima S., Yamamoto H., 2006. Synthesis of hydratalcite-like materials from various wastes in aluminum regeneration process. Resources Processing 53: 6-11.

Okamoto K., Iyi N., Sasaki T., 2007. Factors affecting the crystal size of the MgAl-LDH (layered double hydroxide) prepared by using ammonia-releasing agents. Applied Clay Science 37: 23-31.

Othman M.R., Rasid N.M., Fernando W.J.N., 2006. Effects of thermal treatment on the micro-structures of co-precipitated and sol-gel synthesized (Mg-Al) hydrotalcites. Microporous and Mesoporous Materials 93: 23-28.

Pérez Bernal M.E., Ruano-Casero R.J., Benito F., Rives V., 2009. Nickel-aluminum layered double hydroxides prepared via inverse micelles formation. Journal of Solid State Chemistry 182: 1593-1601.

Pérez-Ramírez J., Mul G., Kapteijn F., Moulijn J.A., 2001. In situ investigation of the thermal decomposition of Co-Al hydrotalcite in different atmospheres. Journal of Materials Chemistry 11: 821-830.

Santini T.C., Fey M.V., 2012. Synthesis of hydrotalcite by neutralization of bauxite residue mud leachate with acidic saline drainage water. Applied Clay Science 55: 94-99.

Schulze K., Makowski W., Chyzy R., Dziembaj R., Geismar G., 2001. Nickel doped hydrotalcites as catalyst precursors for the partial oxidation of light parafins. Applied Clay Science 18 (1-2): 59-69.

Shannon R.D., 1976. Revised effective ionic radii and systematic studies of interatomic distances in halides and chalogenides. Acta Crystallographica section A. 32(5): 751-767.

Stanimirova T.S., Vergilov I., Kirov G., Petrova N., 1999. Thermal decomposition products of hydrotalcite-like compounds: low-temperature metaphases. Journal of Materials Science 34: 4153-4161.

Vágvölgyi V., Palmer S.J., Kristóf J., Frost R.L., Horváth E., 2008. Mechanism for hydrotalcite decomposition: A controlled rate thermal analysis study. Journal of Colloid and Interface Science 318: 302-308.

Yang W., Kim Y., Liu P.-K.T., Sahimi M., Tsotsis T.T., 2002. A study by in situ techniques of the thermal evolution of the structure of a Mg-Al-CO_3 layered double hydroxide. Chemical Engineering Science 57: 2945-2953.

Yang Z., Choi K.-M., Jiang N., Park S-E., 2007. Microwave synthesis of hydrotalcite by urea hydrolisis. Bulletin of the Korean Chemical Society 28 (11): 2029-2033.

Yang Z., Fischer H., Polder R., 2013. Modified hydrotalcites as a new emerging class of smart additive of reinforced concrete for anticorrosion applications: A literature review. Materials and Corrosion 64 (9999): 1-9.

Table 1 P6 and P9 waste composition (main components) obtained by XRF expressed as oxides, and contents of aluminium nitride present

	XRF (% in mass)								Kjeldhal method (% in mass)
	Al_2O_3	MgO	Fe_2O_3	TiO_2	SiO_2	CaO	BaO	Others	AlN
P6	80.49	1.32	0.93	8.30	2.93	1.64	0.08	4.31	23.6
P9	76.85	4.14	0.38	3.21	2.56	1.96	1.38	9.52	16.0

Table 2 Crystallite size (D) measured by Scherrer equation for the 003 basal reflection, cell parameters (*a* and *c*) calculated by equations reported by Pérez-Ramírez et al. [**Pérez-Ramírez et al., 2001**], Zeta potential (mV).

sample	ratio[1] Mg^{2+}/Al^{3+}	D (Å) [2]	*a* (Å) [3]	*c* (Å) [4]	ZETA POTENCIAL (mV)
2BL	2.16	0.084	3.042	22.891	+39 (±6)
2P6	2.00	0.052	3.039	22.846	+35 (±6)
2P9	1.95	0.060	3.040	22.877	+33 (±4)
3BL	2.98	0.112	3.056	23.379	+43 (±5)
3P6	2.91	0.079	3.048	23.179	+42 (±5)
3P9	2.95	0.131	3.052	23.540	+44 (±4)
4BL	3.94	1.045	3.069	24.066	+40 (±6)
4P6	3.88	0.218	3.063	23.923	+34 (±5)
4P9	3.84	0.324	3.068	23.960	+37 (±6)

[1] experimental, determined by ICP-OES;

[2] $D = \frac{k\lambda}{\beta cos\theta}$ (k=0.9; λ = 1.5418; β = 180·FWHM in degrees; θ = experimental Bragg diffraction angle);

[3] $a = 2 \cdot d(110)$;

[4] $c/3 = ½ [d(003)+2 \cdot d(006)]$

Table 3 Textural characterisation on samples previously outgassed overnight at 300°C.

sample	SSA (m^2/g)	S_{EXT} (m^2/g)	Micropore volume (cm^3/g)	Mesopore volume (cm^3/g)
2BL	144	113	0.013	0.482
2P6	143	113	0.013	0.482
2P9	138	106	0.017	0.245
3BL	134	96	0.017	0.398
3P6	182	100	0.037	0.217
3P9	144	80	0.029	0.193
4BL	118	103	0.006	0.181
4P6	208	202	0.000	0.228
4P9	183	106	0.004	0.199

Table 4 Consumption in mass of HCl and waste per hydrotalcite synthesised as a function of the Mg/Al ratio.

sample	kg of HCl / kg of hydrotalcite	kg of waste consumed / kg of hydrotalcite
2P6	0.76	0.64
2P9	0.71	0.60
3P6	0.57	0.48
3P9	0.54	0.45
4P6	0.45	0.38
4P9	0.42	0.36
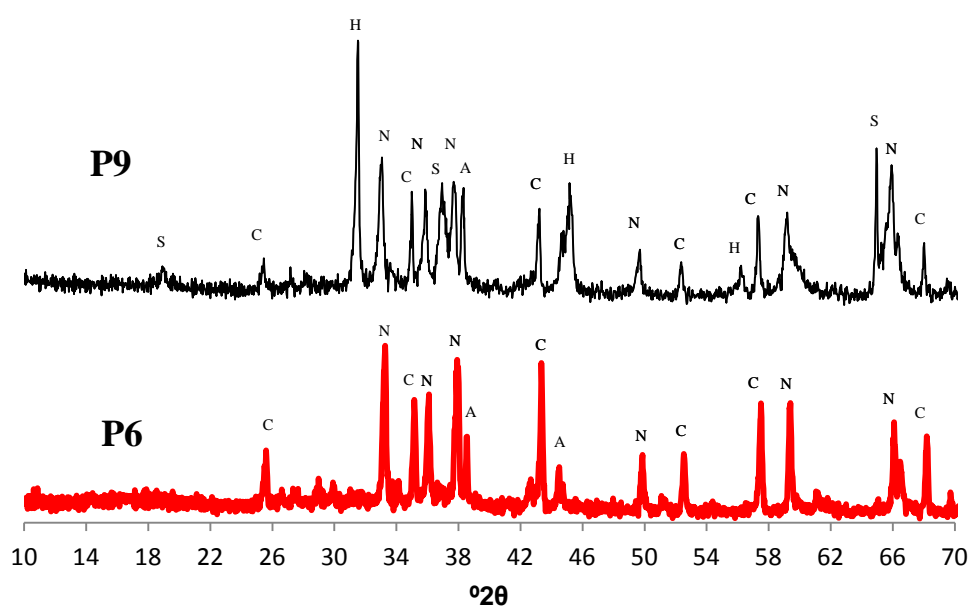
Fig. 1 XRD obtained for wastes P6 and P9. (where A = Al^0; C = Al_2O_3; N = AlN; H = NaCl; S = $MgAl_2O_4$)
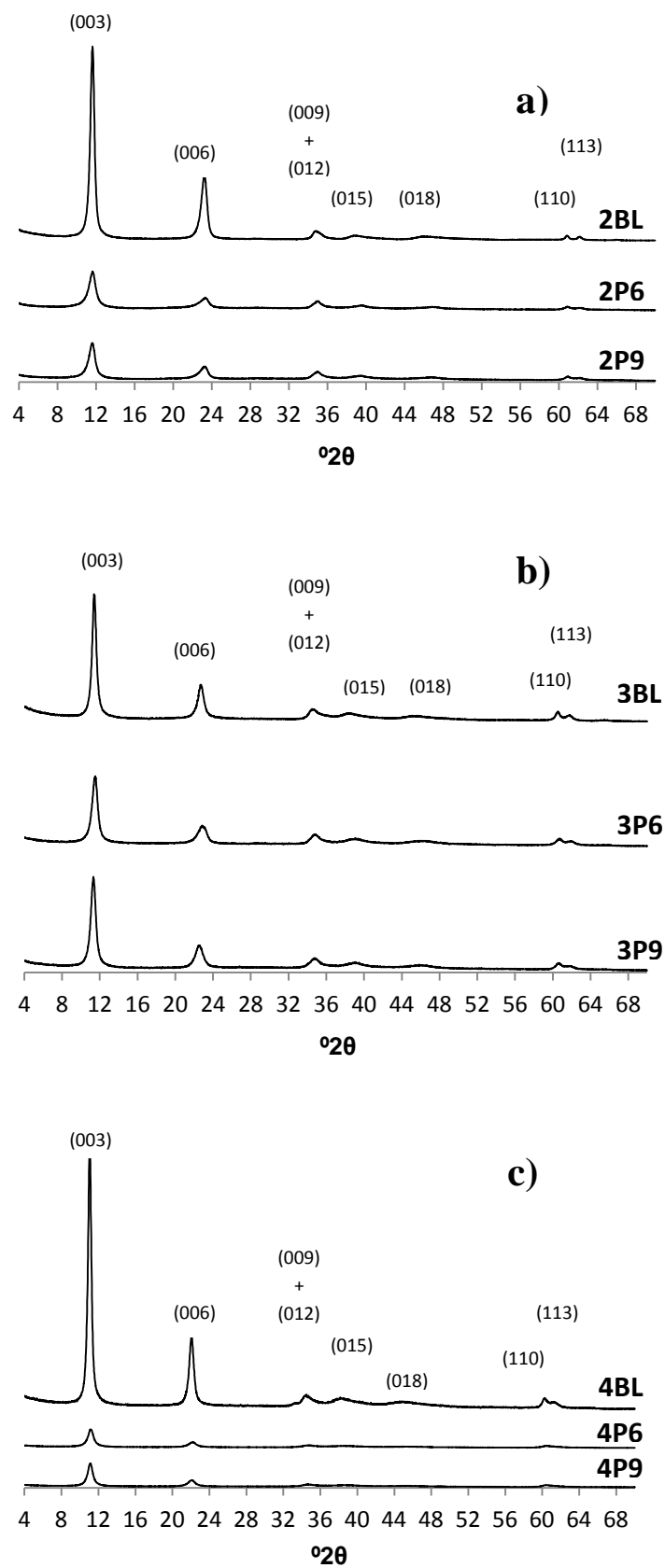
Fig. 2 XRD obtained for blanks (BL) and samples (P6 and P9): a) at ratio Mg/Al 2:1; b) at ratio Mg/Al 3:1; c) at ratio Mg/Al 4:1
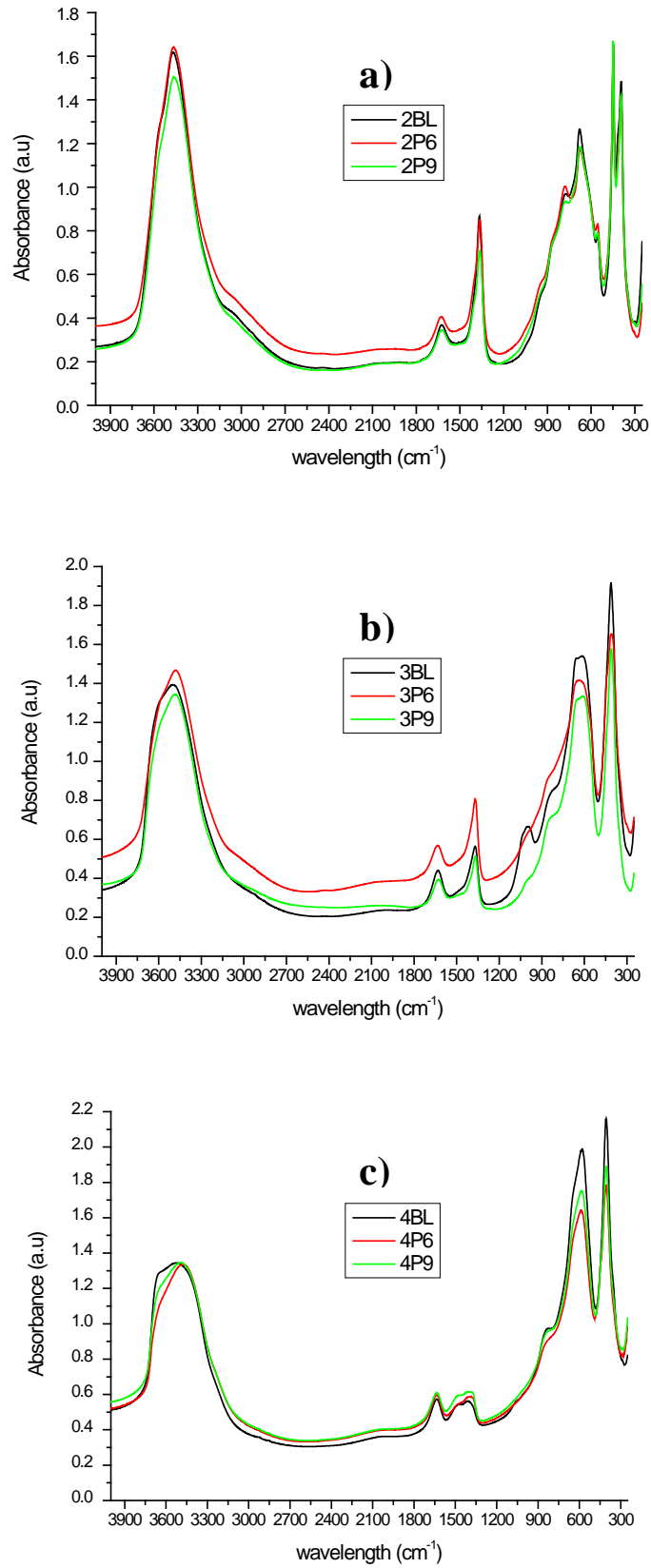
Fig.3 Comparison between FT-IR spectra obtained for blanks (BL) and samples (P6 and P9): a) at ratio Mg/Al 2:1; b) at ratio Mg/Al 3:1; c) at ratio Mg/Al 4:1
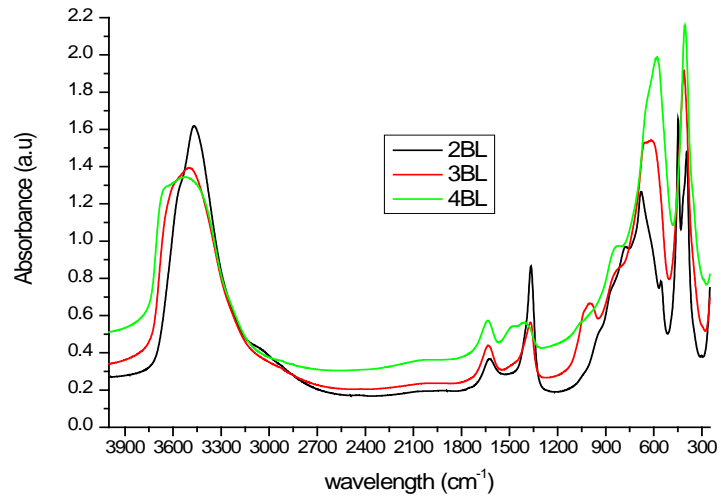
Fig.4 FT-IR spectra obtained for blanks (BL) at ratios Mg/Al 2:1, Mg/Al 3:1 and Mg/Al 4:1
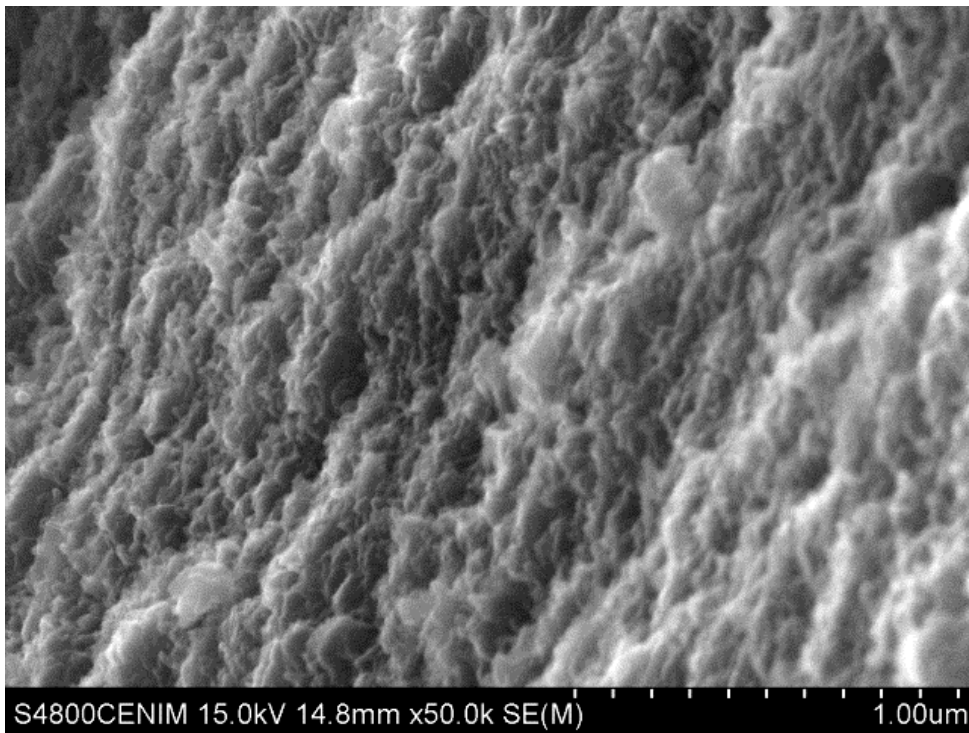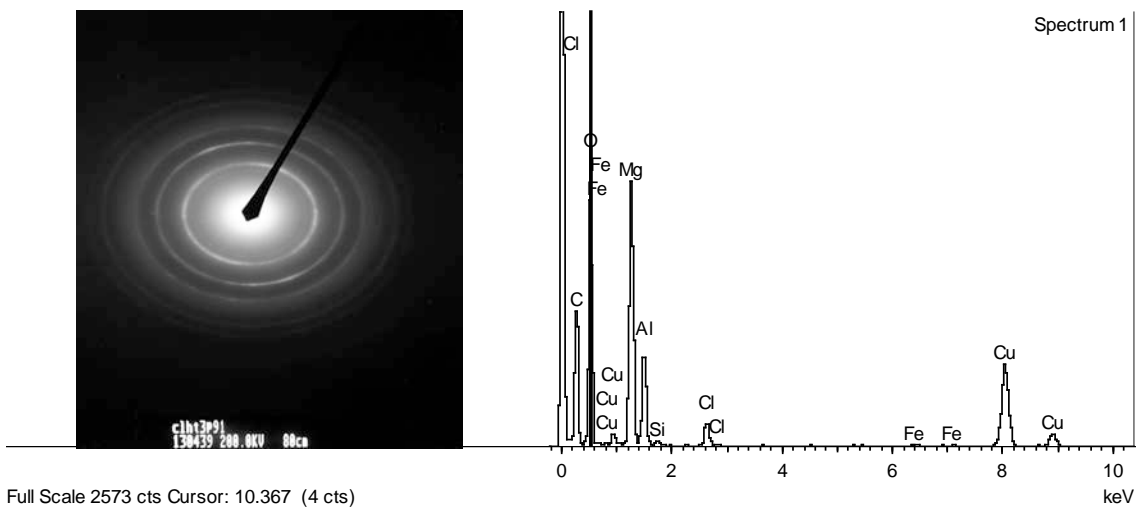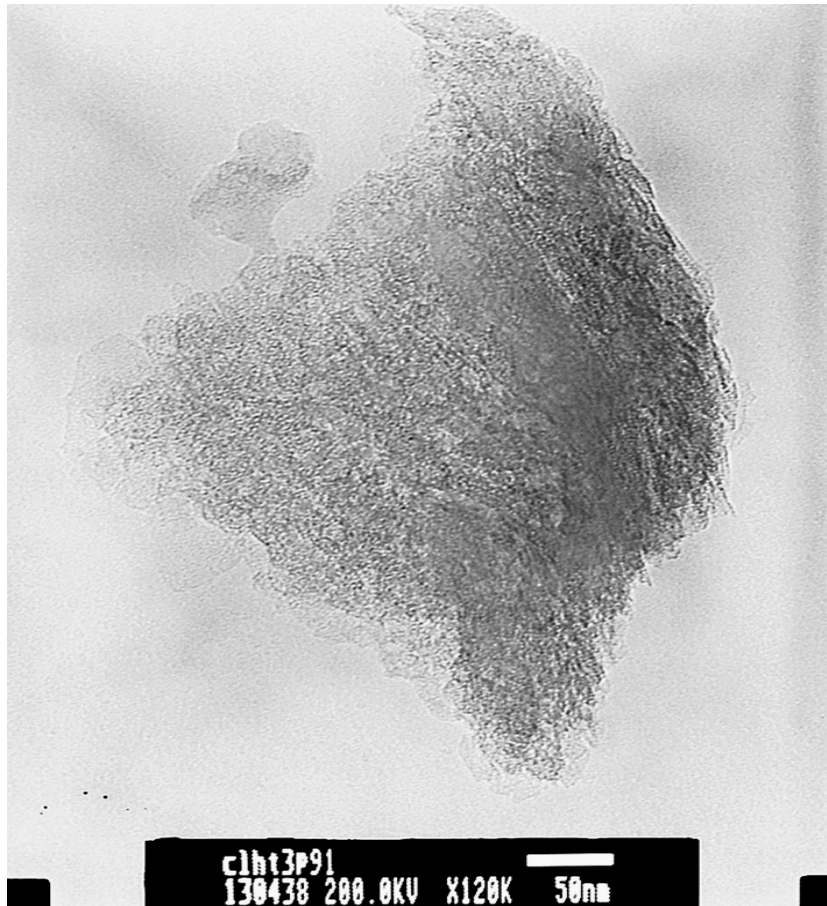

Fig.5 SEM capture for sample 3P6

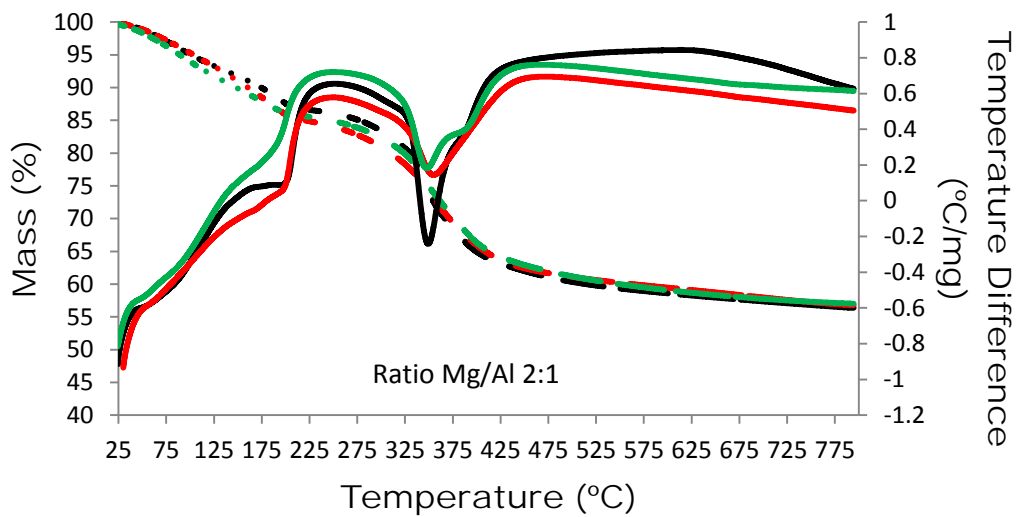Full Scale 2573 cts Cursor: 10.367 (4 cts)

Fig.6 TEM, SAED and EDS captures for sample 3P9
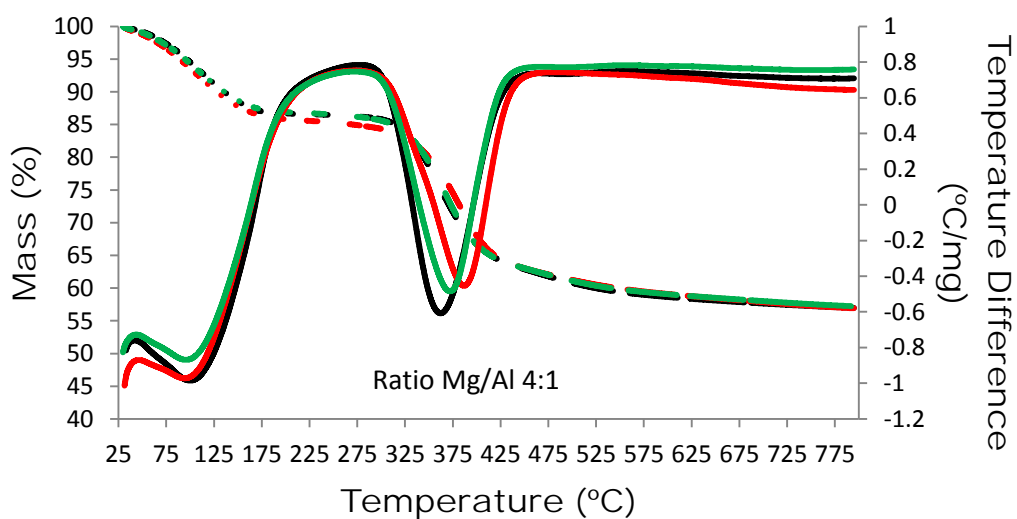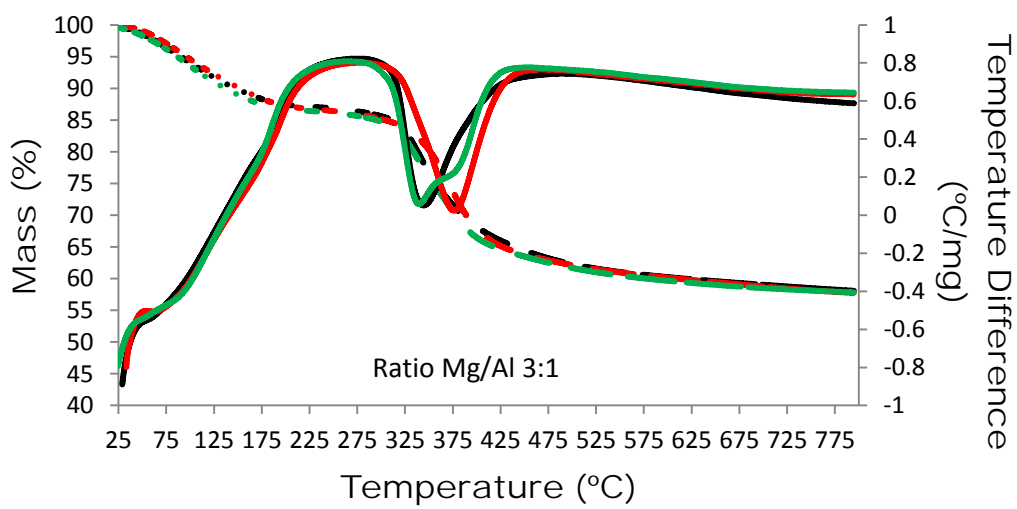
Fig.7 TG (in mass % - dash line) - DTA (in ºC/mg - solid line) for blanks (black), P6
samples (red) and P9 samples (green)

2BL

2P6

2P9
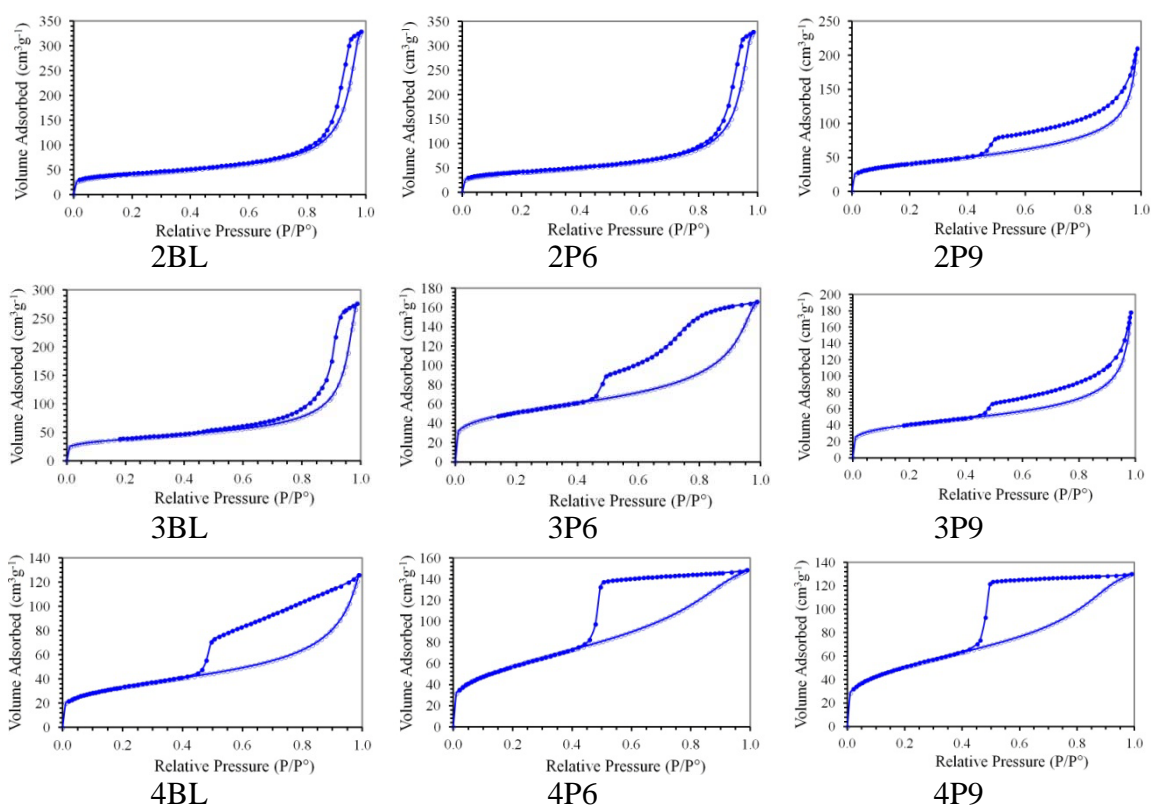

3BL

3P6

3P9

4BL

4P6

4P9

Fig.8 Nitrogen adsorption-desorption isotherms obtained for blanks, P6 samples and P9 samples